Structural Fluctuation and Dynamics of Ribose Puckering in Aqueous Solution from First Principles

Teppei Suzuki,* Hirotaka Kawashima, Hiromi Kotoku, and Takayuki Sota

Integrative Bioscience and Biomedical Engineering, Graduate School of Science and Engineering, Waseda University, 3-4-1 Okubo, Shinjuku, Tokyo 169-8555, Japan

Received: January 27, 2005; In Final Form: April 6, 2005

Using the method of ab initio molecular dynamics, we examine the structural fluctuation and the low-frequency dynamics of β-ribofuranose puckering in aqueous solution. Our analysis suggests that the distance between the anomeric and hydroxymethyl oxygens is a simple relevant geometrical parameter that dynamically correlates with the phase angle in the north region. The time-frequency analysis using the Hilbert−Huang transform also confirms the correlation, and most of the instantaneous frequencies for the phase angle and the above distance are found to be concentrated on the region below about 100 cm^{-1}. Our analysis of ab initio molecular dynamics trajectories suggests that the molecular origin of the hydration effects on the low-frequency dynamics of β-ribofuranose puckering is closely related to this correlation and thus primarily attributed to the relatively local interactions among the anomeric and hydroxymethyl oxygens and the surrounding water molecules near them. Additionally, we discuss the difference in the low-frequency dynamics of β-ribofuranose puckering between two hydroxymethyl rotamers.

Introduction

Sugar puckering plays a central role in determining the global structures of nucleic acids because they can be characterized by the two-state (the North−South) model based on the concept of the pseudorotation cycle[1−4] of the five-membered ring. Therefore, a better understanding of the dynamics of sugar puckering in aqueous solution is essential if one wants to get a better insight into the dynamical properties of nucleic acids in aqueous solution. However, even for β-ribofuranose, the underlying mechanism of the hydration effects on the dynamics of the sugar puckering remains incomplete.

Because of the major building block of RNA, ribofuranose and its derivatives have been the subjects of many theoretical and experimental studies.[5−24] In particular, many theoretical efforts[5,7−11] using quantum chemical approaches have been devoted to the structural and conformational properties of furanoses, especially the relationships between puckering phase angle and their structural parameters. There are also quantum chemical calculations of spin−spin coupling constants[8,12,13] and chemical shifts[20] of carbohydrates to give basic information for NMR spectroscopic studies. Indeed, these computational studies provided valuable insights into the dependences of the physical properties on the sugar puckering of the furanose ring; however, these studies did not adequately address the structural fluctuation and the low-frequency dynamics of sugar puckering in aqueous solution, partly because in these studies,[5,7−13,20,21] one endocyclic torsion angle is normally fixed at zero degrees in the optimization of geometries. Besides, these kinds of approaches often encounter difficulties in modeling the effects of solvent water molecules.

Therefore, in this paper we investigate how the hydration of β-ribofuranose affects the structural fluctuation and the low-frequency dynamics of β-ribofuranose puckering. To deal with this problem, we use the ab initio molecular dynamics (MD) method[25] because it provided an accurate description of liquid water,[26] which would in turn lead one to expect reasonable descriptions of the sugar-oxygen−water-oxygen interactions and the flexible furanose ring. In addition, since in the environment of the dynamic hydrogen bond (H-bond) network of liquid water, ribofuranose puckering fluctuates within the conformational families that can be mapped onto the pseudorotation cycle,[1−4] a kind of temporal descriptor should be needed for an appropriate analysis of the structural and conformational parameters obtained by our MD trajectories. With this perspective, we use a recently developed time-frequency analysis technique proposed by Huang et al.,[27] called the Hilbert−Huang transform (HHT). One of the merits of this method for our present analysis is that it allows us to describe the fluctuation of β-ribofuranose puckering in terms of the instantaneous frequencies and amplitudes with high time resolution, which could help us to detect their changes resulting from molecular-level events that are probably linked to the ribofuranose−water interaction.

This paper is organized as follows. In the second section, we provide our methods including computational details of our simulations, a brief reminder of pseudorotation parameters,[1−4] and a basic idea of the HHT.[27] In the third section, after we establish that the puckering phase angle and the distance between the anomeric and hydroxymethyl oxygens are dynamically correlated, we scrutinize how the hydration of β-ribofuranose affects the structural fluctuation and the low-frequency dynamics of puckering phase angle. In the last section, we summarize the conclusions.

Simulation Models and Methods. The β-ribofuranose−water system was modeled in a cubic supercell of side 12.68 Å with periodic boundary conditions, containing sixty water molecules and one β-ribofuranose. The conformers of β-ribofuranose considered in the present work were the north (N) forms (see Figure 1c) of the two distinct orientations of the

* Corresponding author. E-mail: teppei_suzuki@moegi.waseda.jp.

10.1021/jp050475i CCC: $30.25
Published on Web 06/10/2005

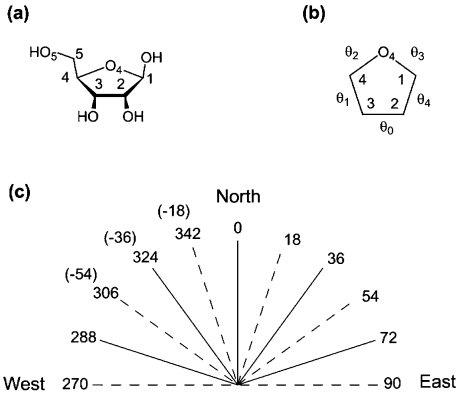

Figure 1. The atom labeling scheme for β-ribofuranose (a), the definition of the five torsion angles $\theta_0-\theta_4$ in the five-membered ring (b), and the pseudorotation cycle in the north region (c). Throughout the paper, the hydroxymethyl rotamers are defined by the O4−C4−C5−O5 torsion angle, which can be $\approx+60°$ (G^+ or *gt*) or $-60°$ (G^- or *gg*), or 180° (T or *tg*). The angles θ_0, θ_1, θ_2, θ_3, and θ_4 are the C1−C2−C3−C4, C2−C3−C4−O4, C3−C4−O4−C1, C4−O4−C1−C2, and O4−C1−C2−C3 torsion angles, respectively, throughout the paper.

hydroxymethyl group: G^+ and G^- (for the definition, see the caption of Figure 1). Our ab initio MD simulations were performed using CPMD code.[28] The Car−Parrinello equations of motion[29] were integrated using a time step of 0.0968 fs and a fictitious electronic mass of 400 au.[30] The mass of deuterium was not used for hydrogen. The electronic structure calculations were carried out in the framework of the Kohn−Sham density functional theory,[31] and the gradient-corrected BLYP functional[32] was used. The valence electronic wave functions were expanded up to 70 Ry, and the valence-core interactions were treated by norm-conserving pseudopotentials by Goedecker, Teter, and Hutter.[33] Only the Γ point was used to sample the Brillouin zone. After an initial equilibration phase of 3 ps using the Nosé−Hoover chain thermostat method[34] to control the ionic temperature at 300 K, data were collected for a microcanonical MD run of 6 ps, in which the average temperatures for the simulations of the G^- and G^+ rotamers were 296 and 297 K, respectively. In these simulations, the average dihedral angles of the hydroxymethyl group for G^- and G^+ were $-68.5 \pm 11.3°$ and $67.0 \pm 7.9°$, respectively, indicating that neither of the two simulations underwent the reorientation of the hydroxymethyl group. These are the same simulations as in our previous work.[35] In the simulations of β-ribofuranose in the gas phase, after all water molecules in the cubic supercell were removed, the simulations of the G^- and G^+ rotamers at low temperature (20 K) were performed in the same way.

To describe sugar puckering of the five-membered ring, we used one of pseudorotation parameters, phase angle *P*. There are two definitions for the pseudorotation parameters: the one by Altona−Sundaralingam[1] and the other by Cremer−Pople.[2] But later Rao, Altona, and Sundaralingam[3] showed that these two definitions are almost equivalent. In the present work, phase angle *P* was calculated by the formula by Altona and Sundaralingam,[1,3]

$$P = \tan^{-1}\left[\frac{(\theta_2+\theta_4)-(\theta_1+\theta_3)}{2\theta_0(\sin(\pi/5)+\sin(2\pi/5))}\right] \qquad (1)$$

where $\theta_0-\theta_4$ are the five endocyclic torsion angles in the furanose ring (for the definition of these angles, see Figure 1). Since *P* has values between −90 and 90° within the standard definition for the arctangent function, if one wants *P* to have values between 0 and 360°, *P* should be replaced by

$$P' = \begin{cases} (P+360°) \bmod 360° & (\theta_0 \geq 0) \\ P+180° & (\theta_0 < 0) \end{cases} \qquad (2)$$

Note that if θ_0 is positive, puckering conformation is in the N region whereas if θ_0 is negative, puckering conformation is in the south (S) region.

In our analysis of the structural parameters of β-ribofuranose obtained by the ab initio MD simulations, in particular, we used the HHT,[27] which combines empirical mode decomposition[27] (EMD) and the Hilbert transform. This technique has recently emerged as a useful tool for analyzing nonstationary signals and has been applied to a variety of systems including fluid mechanics,[36] chaotic systems,[37] Brownian and molecular dynamics,[38] and epidemiology.[39] In the EMD method by Huang et al.,[27] an original signal is decomposed into several intrinsic mode functions (IMFs) and a residue, using a shifting process. The aim of the process is to make the instantaneous frequencies of IMFs well defined for the Hilbert analysis. In the process, we used the stopping criteria proposed by Huang et al.[36] and cubic spline functions to define extrema. According to the notations by Huang et al.,[27,36] an IMF that is first decomposed by the shifting process is called c_1. Hereafter, we call c_1 the first IMF. Similarly, we call c_2, c_3, c_4, etc., the second, third, fourth, etc., IMFs. After the shifting process, the time-frequency energy spectrum, which will be called the Hilbert−Huang spectrum, was computed using the instantaneous frequencies and amplitudes of all IMFs. Following the original papers,[27,36] we used squares of amplitudes as energies.

Results and Discussion

Correlation between the Phase Angle and the O1−O5 Distance for the N Conformer. In previous work using quantum chemical approaches,[5,7−13,20,21] one endocyclic torsion angle is fixed at zero degrees in optimizing geometries (in the case of planar forms, two endocyclic torsion angles are fixed at zero degrees). For example, for ^{3}E (i.e., $P = 18°$ or so-called *C3′-endo*) puckering, the C4−O4−C1−C2 torsion angle (θ_3) is fixed at zero degrees, whereas for $_2$E (i.e., $P = 342°$ or so-called *C2′-exo*) puckering, the C3−C4−O4−C1 torsion angle (θ_2) is fixed at zero degrees. Computational studies using this approximation[5,7−13, 20, 21] provided valuable insights into the dependences of the many properties on the pseudorotation cycle; however, since the sugar puckering of β-ribofuranose in aqueous solution fluctuates within the conformational families in the pseudorotation cycle, these approaches cannot analyze the structural fluctuation and the low-frequency dynamics of β-ribofuranose that is embedded in the dynamic H-bond network of liquid water.

Therefore, to begin with, we checked out the average values and the standard deviations for the endocyclic torsion angles (i.e., θ_0, θ_1, θ_2, θ_3, and θ_4) and the phase angle obtained from the aqueous-phase simulations. In the simulations of the G^- and G^+ rotamer, the average phase angles were $355.2 \pm 21.7°$ and $340.0 \pm 18.9°$, respectively, and the average values for θ_2 were 9.0 and −1.1, respectively. While these roughly correspond to $_2$E ($P = 342°$; $\theta_2 = 0°$), the standard deviations for θ_2 and θ_3 were larger than the ones for the other endocyclic angles (Table 1), indicating that θ_2 and θ_3 were more flexible than the other endocyclic angles in our simulations of the N conformers. This is because in our simulations *P* fluctuated the region between about 315 (i.e., −55) and 18° (see also Figure 2).

TABLE 1: Average Values (deg) and the Standard Deviations (deg) for θ_0, θ_1, θ_2, θ_3, and θ_4 Obtained from the Aqueous-Phase Simulations of the North Conformer of β-Ribofuranose

	G^- rotamer[a]		G^+ rotamer[b]	
torsion angle[c]	average	standard deviation	average	standard deviation
θ_0	36.9	6.7	33.6	6.2
θ_1	−28.8	10.1	−20.9	9.7
θ_2	9.0	13.9	−1.1	12.1
θ_3	14.7	13.6	23.1	11.0
θ_4	−31.9	9.3	−35.2	7.0

[a] The average phase angle was 355.2 ± 21.7. [b] The average phase angle was 340.0 ± 18.9. [c] For the definition of θ_0, θ_1, θ_2, θ_3, and θ_4, see the caption of Figure 1.

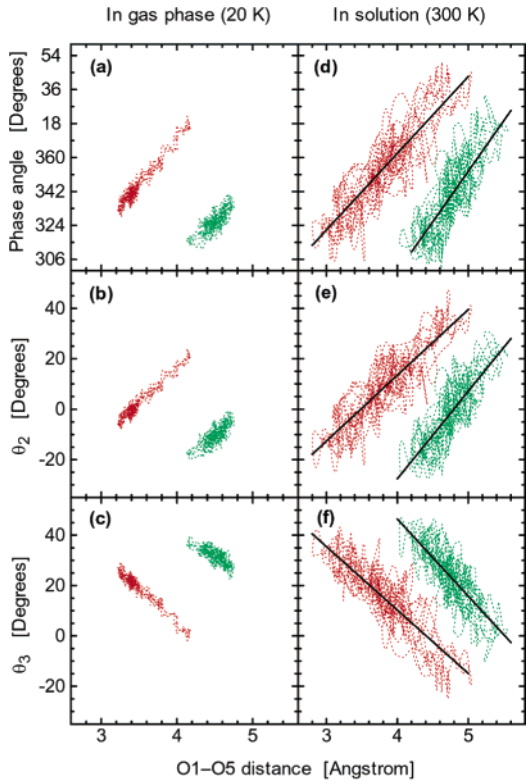

Figure 2. Plots of the phase angle (top panel), θ_2 (central panel), and θ_3 (bottom panel) as a function of the O1−O5 distance in the gas (20 K) (left: a−c) and aqueous (300 K) (right: d−f) phases, respectively. For the definitions of θ_2 and θ_3, see Figure 1. Red- and green-dotted lines denote G^- and G^+, respectively. Fitted linear lines in parts d−f were obtained by the method of least squares.

Besides, the standard deviations of the five endocyclic torsion angles ranged from about 6 to 14° (Table 1), indicating that all endocyclic torsion angles moderately fluctuated. Moreover, as Altona and Sundaralingam originally pointed out, equilibrium like *C2′-exo*↔*C3′-endo* (or identically, $_2E \leftrightarrow {}^3E$) is misleading, because these two forms are not separated by a potential energy barrier, but rather part of an allowed region of the pseudorotation cycle.[4] That is, nomenclatures such as twists or envelopes are only idealized forms, and they are just reflections of the signs of endocyclic torsion angles (either positive or negative, or zero).[4] The above observations indicate that the approximation used by the quantum chemical approaches is not adequate for the aim of our present study, which somewhat justify our use of ab initio MD simulations based on density functional theory to investigate the structural fluctuation and the low-frequency dynamics of β-ribofuranose puckering in aqueous solution.

TABLE 2: Correlation Coefficients between the Phase Angle and the Distances between All Pairs of β-Ribofuranose Oxygens

	in the aqueous phase		in the gas phase	
pair	G^- rotamer	G^+ rotamer	G^- rotamer	G^+ rotamer
O1−O2	−0.36	−0.12	−0.58	0.01
O1−O3	0.44	0.16	0.81	−0.12
O1−O4	−0.01	−0.22	−0.53	−0.08
O1−O5	0.87	0.80	0.97	0.76
O2−O3	0.07	0.06	0.02	0.49
O2−O4	0.67	0.54	0.88	0.36
O2−O5	0.28	−0.29	0.75	−0.47
O3−O4	0.32	0.39	0.72	0.75
O3−O5	−0.33	−0.36	−0.82	−0.48
O4−O5	−0.32	−0.04	−0.02	0.00

When ribose oxygens are embedded into dynamic H-bond network of liquid water, ribose oxygens may play a role in the low-frequency dynamics of sugar puckering in aqueous solution. With this perspective, we attempted a rather different approach: we investigated the correlation coefficients between the phase angle and the distances between all 10 pairs of β-ribofuranose oxygens obtained from the aqueous-phase simulations. First, we found that the phase angle was highly correlated with the O1−O5 distance (G^-, 0.87; G^+, 0.80) among the distances between all pairs of β-ribofuranose oxygens (Table 2). Then, we found the second highest correlation of the phase angle was between the O2−O4 distance (G^-, 0.67; G^+, 0.54); however, the correlation coefficients of the phase angle with the distances of the other pairs of β-ribofuranose oxygens were found not to be so high (Table 2). Additionally, we calculated the correlation coefficients for the gas-phase simulations. In particular, the phase angle of the G^- rotamer was correlated with several other pairs of β-ribofuranose distances (the exceptions were between the O2−O3 and O4−O5 distances, see Table 2). This suggests that in going from the gas to aqueous phase, the correlations of the phase angle with some of these distances were lost, because of thermal fluctuation and intermolecular hydrogen bonds with surrounding water molecules. In other words, the high correlation of the phase angle with the O1−O5 distance was maintained, even in the environment of the dynamic H-bond network of liquid water. Besides, we found that the correlation of the phase angle with the O1−O5 distance of the G^- rotamer was slightly higher than that of the G^+ rotamer (Table 2), which may have implications for understanding the dynamics of RNA.

Motivated by the above finding, we further quantitatively investigated the correlation between the phase angle and the O1−O5 distance. As one would expect from the high correlations in Table 1, the phase angle almost linearly correlates with the O1−O5 distance in the gas phase (Figure 2a). The correlation holds for the aqueous phase (Figure 2d); but the plots were scattered owing to thermal fluctuation and intermolecular H-bonds between β-ribofuranose and water molecules, compared with the gas-phase simulations. Similarly, θ_2 and θ_3 also linearly correlates with the O1−O5 distance (θ_2, Figure 2b and e; θ_3, Figure 2c and f). This is not surprising because the motions of endocyclic torsion angles and puckering phase angle are correlated: endocyclic torsion angles are given by[1,3]

$$\theta_j = \theta_m \cos(P + j4\pi/5) \quad (3)$$

where θ_m is puckering amplitude and $j = 0$, 1, 2, 3, and 4. When the phase angle is in the N region, θ_2 and θ_3 are roughly given by

$$\theta_2 = \theta_m \cos(P + 8\pi/5) = \theta_m \sin(P + \pi/10) \approx \theta_m (P + \pi/10) \quad (4)$$

$$\theta_3 = \theta_m \cos(P + 12\pi/5) = -\theta_m \sin(P - \pi/10) \approx -\theta_m (P - \pi/10) \quad (5)$$

where in this case $-\pi/2 < P < \pi/2$. Since θ_m is always positive,[1,3] the above equations and the correlation between the phase angle and the O1−O5 distance explain that when the O1−O5 distance becomes longer, θ_2 and P increase whereas θ_3 decreases (Figure 2). More quantitatively, for the G^- and G^+ rotamers, respectively, θ_2 increases at a rate of about 26 and 34 deg/Å, whereas θ_3 decreases at a rate of about 25 and 31 deg/Å (Figure 2). These indicate that if puckering conformation is in the N region, the phase angle and the O1−O5 distance are well correlated: in the N region, when the O1−O5 distance becomes shorter, the phase angle rotates anticlockwise in the pseudorotation cycle (Figure 1c) whereas when the O1−O5 distance becomes longer, the phase angle rotates clockwise. Note that this correlation is independent of whether O1 and O5 form an intramolecular H-bond between them, because the correlation holds even for longer O1−O5 distances (see Figure 2d−f). In addition, this correlation may have implications for the transitions between the N and S conformers in aqueous solution.

Whereas the correlation between the phase angle and the O1−O5 distance was also checked out by comparing the time series (Figure 3), this kind of correlation between the O1−O5 distance and the C4−O4−C1 angle appeared less obvious (Figure 3). One of the reasons is that the motion of the C4−O4−C1 angle is normally much faster than pseudorotational motion and the low-frequency motion of the O1−O5 distance (in fact, more than 70% of the frequencies for the C4−O4−C1 angle were located at the region above 500 cm^{-1}). In addition, we calculated the correlation coefficients between the phase angle and the angles belonging to the five-membered ring (i.e., the C2−C3−C4, C3−C4−O4, C4−O4−C1, O4−C1−C2, and C1−C2−C3 angles) and checked that the correlations of the phase angle with these distances were fairly small in the aqueous-phase simulations (Table S1 in Supporting Information). Moreover, we found that moderate correlations of the phase angle with some of the above angles in the gas phase were lost in going from the gas to aqueous phase (Table S1 in Supporting Information), partly because of thermal fluctuation and the intermolecular interactions between the solutes and the surrounding water molecules. Certainly, it was reported[40,41] that the C4−O4−C1 angle periodically depends on puckering phase angle; however, this dependence prove[40,41] to be highly scattered by thermal fluctuation and therefore can be detectable only when puckering phase angle changes its conformation from the N to S region or vice versa. In our simulations, the average values of the C4−O4−C1 angle were 108.9 ± 2.6° (G^-) and 108.8 ± 2.8° (G^+), implying that the possible correlations could not be detected by these deviations. The ensembles obtained by our simulations, which were limited to the N region because of the use of ab initio MD approach, did not allow us to further examine such dependence.

While it was reported[5,7−11] that the bond distances and the angles belonging to the five-membered rings of furanoses correlate with their phase angles, these kinds of correlations obtained by quantum chemical approaches are limited to static properties, and therefore these correlations do not necessarily mean that they are *dynamically* correlated with the phase angle. From molecular-vibrational point of view, since stretching vibrational frequencies of C−C, C−O, and C−H bonds are much higher than the low-frequency dynamics of sugar puckering, whether they are dynamically correlated with the phase angle is less obvious; indeed, by calculating the correlation coefficients between the phase angle and the distances belonging to the five-membered ring (i.e., the O4−C1, C1−C2, C2−C3, C3−C4, and C4−O4 distances), we found that the correlations of the phase angle with these distances were considerably small (Table S2 in Supporting Information). Thus, if one wants to study the hydration effects on the low-frequency dynamics of sugar puckering, the above correlations are likely to be of secondary importance. Furthermore, the correlation coefficients of the phase angle with the torsional motions of the hydroxyl groups and the hydroxymethyl ones of β-ribofuranose were fairly small (Table S3 in Supporting Information). Our analysis suggests that the O1−O5 distance is a simple relevant geometrical parameter that dynamically correlates with the phase angle of the N conformer of β-ribofuranose in aqueous solution. This implies that the correlation between the phase angle and the O1−O5 distance plays a role in the structural fluctuation and the low-frequency dynamics of the sugar puckering of β-ribofuranose when the molecule is embedded in the H-bond network of liquid water.

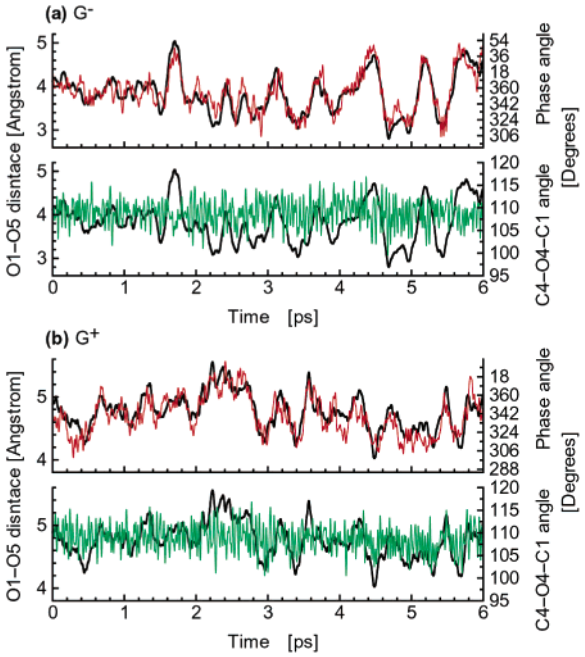

Figure 3. Time evolution of the phase angle (red), the C4−O4−C1 angle (green), and the O1−O5 distance (black) for G^- (a) and G^+ (b).

Hydration Effects on the Low-Frequency Dynamics of the Sugar Puckering. After we had established that the phase angles were dynamically correlated with the O1−O5 distances, we investigated how the hydration of β-ribofuranose affected the low-frequency dynamics of the two rotamers of our simulations. In our simulation of the G^- rotamer in aqueous solution, we observed intra- and intermolecular H-bonds involving O1 and O5: Forming the H-bonds to O5 and O1 as proton acceptor and donor, respectively, a water molecule in the first hydration shell was first located between O5 and O1 (Figure 4a). In this configuration, the O1−O5 distance was 3.99 Å and the phase angle was 7°. Because of thermal fluctuation, one of the hydrogen atoms of the first-hydration-shell water sometimes formed bifurcated H-bonds to the O1 and O4 (snapshot not shown), and then the H-bond to O1 was broken and re-formed to O4 (Figure 4b). In the configuration of Figure 4b, the O1−O5 distance was 4.89 Å and the phase angle was 36°. From the

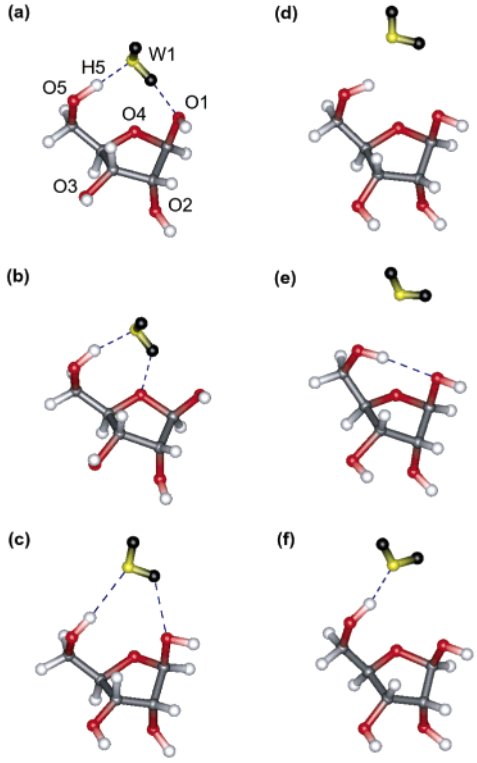

Figure 4. Sampled snapshots taken from the ab initio MD simulation of the G^- rotamer undergoing the inter- and intramolecular hydrogen bonds: t = about 1.30 (a), 1.74 (b), 2.08 (c), 2.16 (d), 2.28 (e), and 3.82 ps (f). The puckering phase angles and the O1−O5 distances in the above configurations are the following: 7°, 3.99 Å (a); 36°, 4.89 Å (b); 353°, 3.60 Å (c); 352°, 3.61 Å (d); 329°, 3.17 Å (e); 354°, 3.72 Å (f), respectively. The first-hydration-shell water (W1) that moderately affected the structural fluctuation of the sugar puckering of the G^- rotamer is shown and the other water molecules are omitted. The atomic labeling scheme is given only in (a). In β-ribofuranose molecule, carbon atoms are colored by gray, oxygens red, and hydrogens white; while in the first-hydration-shell water (W1), the oxygen is colored by yellow and the hydrogens black. Note that these snapshots do not give a complete picture for the observed hydrogen bond dynamics, which was more complex owing to thermal fluctuation. For more detailed information about hydrogen bond dynamics, see Figure 5. For the molecular visualization, we used gOpenMol, version 2.32 (ref 52), throughout the paper.

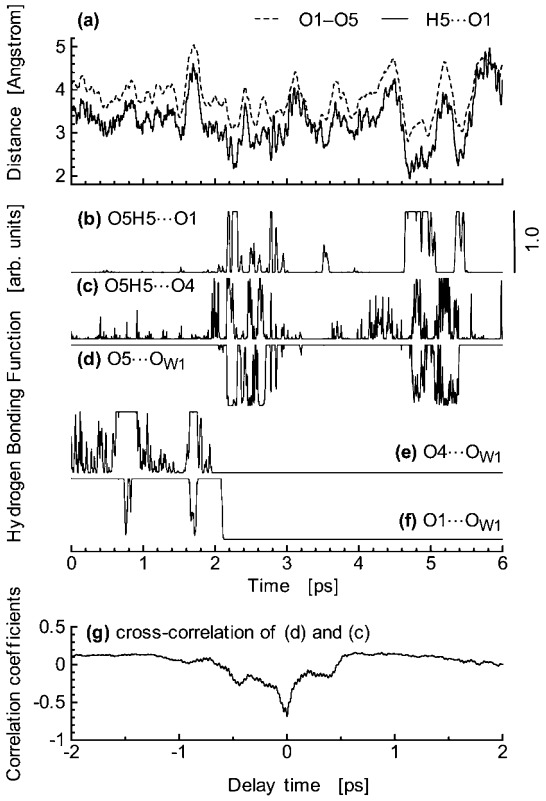

Figure 5. Time series of the O1−O5 (solid line) and H5···O1 (dashed line) distances (a), the hydrogen bonding functions for the intramolecular hydrogen bonds (b, O5H5···O1; c, O5H5···O4), those of the intermolecular hydrogen bonds (d, O5···O_{W1}; e, O4···O_{W1}; f, O1···O_{W1}), and the cross-correlation function (g) of the hydrogen bonding functions for O5···O_{W1} and O5H5···O4 hydrogen bonds. All data were obtained from the simulation of the G^- rotamer in aqueous solution. The notations are the same as shown in Figure 4.

configuration of Figure 4a to that of Figure 4b, the phase angle increased about 30°, indicating that the break of the O1···W1 intermolecular H-bond made the O1−O5 distance longer and the phase angle rotate clockwise in the pseudorotation cycle. The configuration shown in Figure 4b did not appear stable and returned to configurations similar to that of Figure 4a. After these kinds of fluctuations, the water molecule moved away from O1 and O5 almost simultaneously (Figure 4c and 4d). Then β-ribofuranose formed an intramolecular H-bond (see Figure 4e; in this configuration, the O1−O5 distance was 3.17 Å and the phase angle was 329°). This means that the formation of the intramolecular H-bond between O1 and O5 (Figure 4e) made the phase angle rotate anticlockwise in the pseudorotation cycle. This intramolecular H-bond was repeatedly formed and broken, and returned to form an intermolecular H-bond (Figure 4f). The above observations suggest that in our simulation of the G^- rotamer, the fluctuations of the O1−O5 distance and the phase angle were created by the interplay between the intra- and intermolecular H-bond dynamics owing to the interaction between β-ribofuranose and the first-hydration-shell water molecule.

Next, we further examined the H-bond dynamics involving these events. Looking at the time series of the O1−O5 and H5···O1 distances of G^-, we found that the O1−O5 distances ranged from about 2.8 to 5.0 Å and that the time evolution of the H5···O1 distance correlated with that of the O1−O5 one (Figure 5a). These suggest that the intramolecular H-bond between O1 and O5 was closely related to the motion of the O1−O5 distance, rather than the C4−C5−O5−H5 rotational motion. More quantitative discussion about the H-bond dynamics can be given by a function that is unity if a particular pair of oxygens forms an H-bond and decays to zero as they deviate from a predefined condition for H-bonds. Hereafter we refer to this function as an *H-bonding function*. Our H-bonding function is similar to that of ref 42 and defined by $H(t) = R(t)A(t)$, where $R(t)$ is unity if $d(t) \le d_c$ and otherwise $\exp[-(d(t) - d_c)^2/2\sigma_r^2]$, while $A(t)$ is unity if $\theta(t) > \theta_c$ and otherwise $\exp[-(\theta(t) - \theta_c)^2/2\sigma_\theta^2]$. Here $d(t)$ and $\theta(t)$ are the instantaneous H···O_A distance and O_D−H−O_A angle, respectively, and in the present work, d_c, θ_c, σ_r, and σ_θ were 2.4 Å, 120°, 0.2 Å, and 10°, respectively. The comparison of the H-bonding function of Figure 4c and the one of Figure 4d implies that intramolecular (Figure 4b and c) and intermolecular (Figure 4d) H-bonds were mutually competitive; in fact, this is supported by the cross-correlation function between the H-bonding functions in Figure 4c and 4d, whose correlation coefficient at the delay time of zero is −0.68 (negative correlation; see Figure 4g). Also, the similar trend is found between Figure 4e and 4f. These mean that in G^- the O1···O5 and O4···O5 intramolecular H-bonds were formed only when the intermolecular H-bond broke and

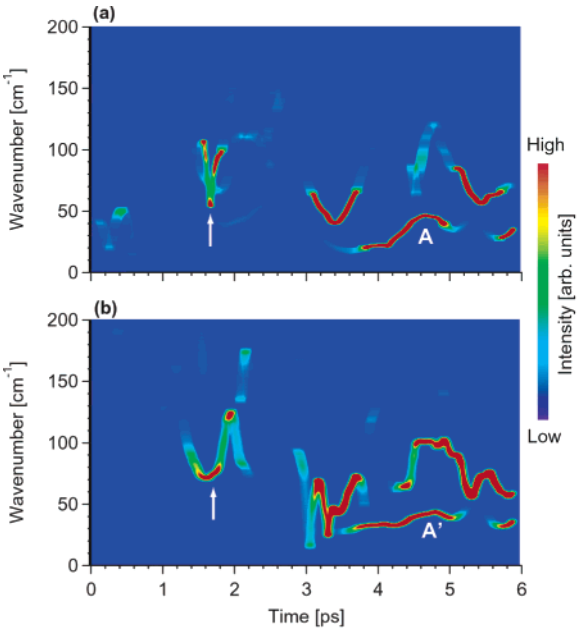

Figure 6. Hilbert−Huang spectra in the 0−200 cm^{-1} region obtained from the time series of the O1−O5 distance (a) and the phase angle (b) for the G$^-$ rotamer in aqueous solution. To make the spectra clearer, we smoothed them using Gaussian functions. Also, we omitted two intrinsic mode functions in which about half the instantaneous frequencies were lower than 20 cm^{-1}. For the full behavior of the intrinsic mode functions labeled by A and A′, see Figure 7c. The arrows correspond to the break of the O1···O$_{W1}$ hydrogen bond and the formation of the O4···O$_{W1}$ hydrogen bond (see in particular at ≈1.7 ps in Figure 5e and 5f).

did not appear stable (the residence times did not exceed about 0.4 ps in the simulation). These kinds of unstable intramolecularH-bonds in the presence of solvent water molecules are consistent with molecular dynamics studies of ribofuranose,[15] deoxyribofuranose,[15] glucopyranose,[43,44] and other sugars[45] in aqueous solution and quantum chemical calculations of glucose−water complexes.[46,47]

The analysis of the Hilbert−Huang spectra of the O1−O5 distance and the phase angle enables us to examine the time evolution of their instantaneous frequencies. Consistent with the previous report[18] by computer simulations of nucleosides, most of the instantaneous frequencies of the pseudorotational motion were lower than ≈100 cm^{-1} (Figure 6b). This holds for the dynamics of the O1−O5 distance (Figure 6a). If we assume that the band centered on ≈160−180 cm^{-1} of liquid water, which is the higher band of the two main ones[26b] of the low-frequency spectral density of liquid water, is associated with the O−O stretching motion,[26b] these imply that the fluctuations of the phase angle and the O1−O5 distance are relatively insensitive to the O−O stretching motions of surrounding water molecules.

Comparing Figure 6a and 6b, we found the similarity between the Hilbert−Huang spectrum for the O1−O5 distance and the one for the phase angle: The peak centered on ≈1.7 ps in 50−100 cm^{-1} in Figure 6a (indicated by the arrow) corresponds to the break of the O1···O$_{W1}$ H-bond and the forming of the O4···O$_{W1}$ H-bond (see in particular at ≈1.7 ps in Figure 5e and 5f). The corresponding peak is found in the similar position in the time-frequency spectrum for the phase angle (see the peak indicated by the arrow in Figure 6b). Furthermore, the comparison of Figures 5a−d and 6 indicates that the forming and breaking of the O1···O5 intramolecular H-bond and the O5···O$_{W1}$ intermolecular H-bond in the last 3 ps is reflected in

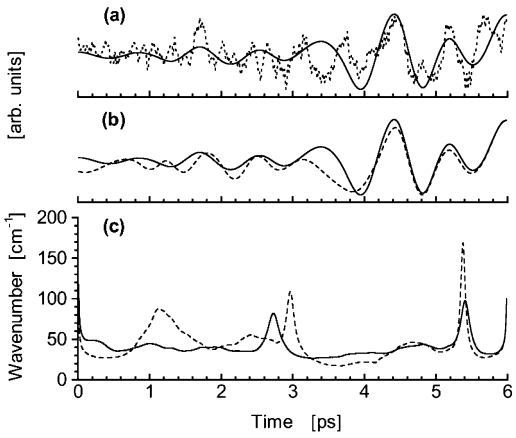

Figure 7. The fifth intrinsic mode function of the phase angle (solid line) compared with the original signal (dotted line) (a), and to the fifth intrinsic mode function of the O1−O5 distance (dashed line) (b) and time-frequency spectra for the phase angle (solid line) and the O1−O5 distance (dashed line) in the 0−200 cm^{-1} region (c). All data were obtained from the simulation of the G$^-$ rotamer. Dashed and solid lines in part c correspond to the peaks labeled by A and A′ in Figure 6, respectively.

the 30−100 cm^{-1} region of the Hilbert−Huang spectra for the phase angle and the O1−O5 distance. These indicate that in our simulation, the dynamics of the O1−O5 distance and the phase angle of G$^-$ was directly created by the forming and breaking of intra- and intermolecular H-bonds.

To check out the connection of the IMFs with the original signal, we compared the time series of the original signal and one of the IMFs, the fifth one obtained from the phase angle. The fifth IMF of the phase angle was found to roughly reproduce the major oscillation of the original signal (Figure 7a). Moreover, the instantaneous amplitude of the IMF in 3−6 ps is higher than that of 0−3 ps (see also A and A′ in Figure 6), which is qualitatively consistent with the behavior of the original signal (Figure 7a). The comparison between the sixth IMF of the phase angle and the O1−O5 distance shows that they were similar to each other (Figure 7b). This is in turn reflected in the similarity in the time evolution of their instantaneous frequencies, which were on average about 40 cm^{-1} (Figure 7c). The relatively rapid changes in the instantaneous frequencies at ≈5.4 ps in Figure 7c (especially dashed line) is considered to be an artifact due to the insufficiency that is related to the EMD. The similarity in the time series of the instantaneous frequencies of the phase angle and the O1−O5 distance indicates their low-frequency correlation.

Now, we turn to the G$^+$ rotamer. First, we compared the autocorrelation functions (ACF) and their spectra of the phase angle between the two rotamers. The striking difference in Figure 8 is that the ACF of G$^-$ is dominated by the oscillation on the time scale of roughly 0.8 ps whereas that of G$^+$ is not.This is also reflected in their spectra: in particular, the power spectrum of G$^-$ is characterized by the three bands at ≈20, 50, and 90 cm^{-1} (see Figure 8b). The comparison suggests a rather difference in the low-frequency dynamics between the two rotamers.

Another way to estimate the spectrum is to calculate the marginal Hilbert−Huang spectrum[27,36]

$$h(\omega) = \int H(\omega,t)dt \qquad (6)$$

where $H(\omega,t)$ is the Hilbert−Huang spectrum. Huang and coworkers[48] pointed out that the HHT tends to detect low-frequency signals more sensitively than Fourier-based methods;

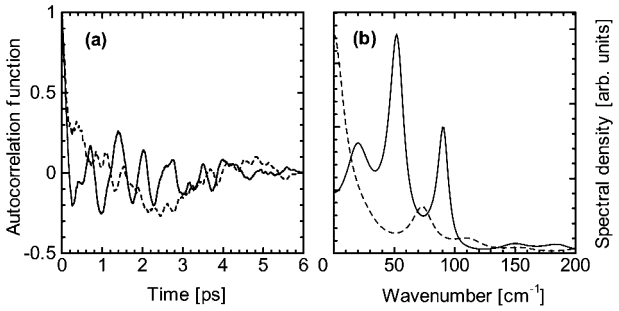

Figure 8. Autocorrelation functions (a) and their spectra (b) of the phase angles of the G^- (solid line) and G^+ (dashed line) rotamers. The spectra were estimated by the maximum entropy method (ref 53).

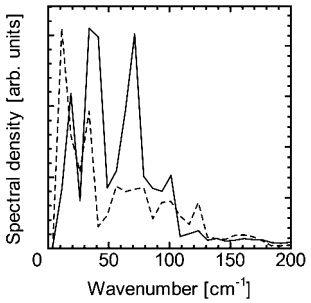

Figure 9. Marginal Hilbert−Huang spectra of the phase angle for G^- (solid line) and G^+ (dashed line) in the 0−200 cm^{-1} region. In calculating the marginal spectra, we omitted the last-decomposed intrinsic mode functions (the seventh and sixth ones for the G^- and G^+ rotamers, respectively), in which about half the instantaneous frequencies were lower than 10 cm^{-1}. To avoid the artifacts owing to the end effect by the spline fitting (ref 36) that might affect the shape of the spectra, we neglected the instantaneous frequencies of the first and last 300 points.

however, we note that the direct correspondence between the marginal Hilbert−Huang spectrum and those of Fourier-based methods is not a priori obvious because the former is just an accumulation of instantaneous frequencies. Nevertheless, the marginal spectrum for G^-, which has three bands centered on ≈20, 35, and 75 cm^{-1}, is found to be similar to the Fourier transform of the ACF (solid lines in Figures 8b and 9). Furthermore, by checking the instantaneous frequencies associated with the decomposed IMFs, we found that the bands at 40−50 cm^{-1} and 60−80 cm^{-1} in the marginal spectrum for G^- (solid line in Figure 9) reflected the contributions from the fifth IMF and the fourth one (of especially the last 3ps), respectively. On the other hand, the marginal spectrum for G^+ is characterized by two bands at 10−20 and 30−40 cm^{-1} and the broad band between 50 and 110 cm^{-1} (dashed line in Figure 9). In G^+, the resemblance between the marginal spectrum (dashed line in Figure 9) and the Fourier transform of the ACF (dashed line in Figure 8b) appears less apparent compared with the case of G^-. One of the reasons for this discrepancy is that the frequency region below ≈20 cm^{-1} (the time scales that are longer than ≈1.7 ps) was difficult to detect when using the ACF for the estimate of the power spectrum, because of the length of our simulation run of 6 ps. However, the two spectra for G^+ (dashed lines in Figure 8b and 9) indicate that the motion of the phase angle of G^+ was concentrated on the region below ≈40 cm^{-1}.

Next, we looked at the Hilbert−Huang spectra and the corresponding IMFs of the phase angle and the O1−O5 distance of G^+. Consistent with the case of G^-, the major low-frequency dynamics of the phase angle occurred at the region below ≈100 cm^{-1} (Figure 10b), which can be also confirmed by the spectra

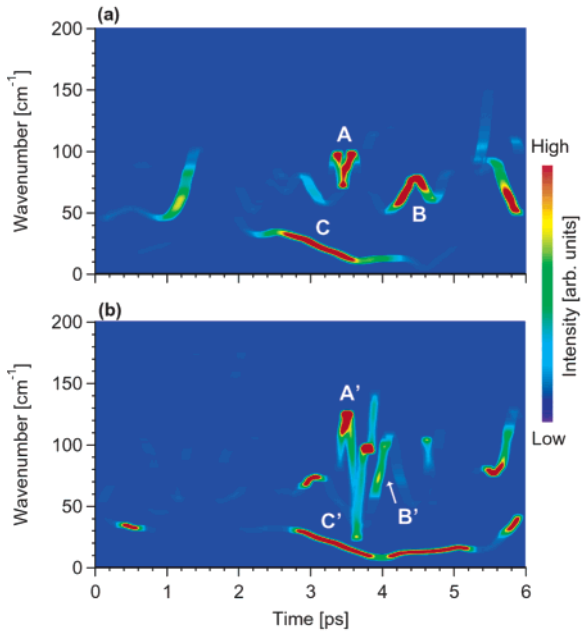

Figure 10. Hilbert−Huang spectra in the 0−200 cm^{-1} region obtained from the time series of the O1−O5 distance (a) and the phase angle (b) for the G^+ rotamer in aqueous solution. To make the spectra clearer, we smoothed them using Gaussian functions. Also, we neglected the intrinsic mode function in which about half the instantaneous frequencies were lower than 10 cm^{-1}. For the intrinsic mode functions labeled by A−C and A′−C′, see Figure 11.

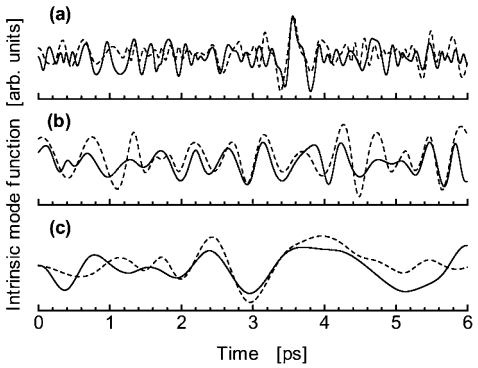

Figure 11. The third, fourth, and fifth intrinsic mode functions of the phase angle (solid line) and the O1−O5 distance (dashed line) (b) for the G^+ rotamer. Dashed and solid lines of parts a−c corresponds to the lines labeled by A−C and A′−C′ in Figure 10, respectively.

in Figures 8b and 9. But the similarity in the Hilbert−Huang spectra between the phase angle and the O1−O5 distance appears slightly inferior (Figure 10) compared with the case of G^- (Figure 6). This is consistent with the fact that the correlation coefficient between the phase angle and the O1−O5 distance for G^+ was slightly lower (about 8%) than that of G^- (see Table 2). Nevertheless, the third through fifth IMF of the two quantities are still similar to each other (Figure 11), suggesting their low-frequency correlation. Looking at the 10−30 cm^{-1} region of the Hilbert−Huang spectra for the phase angle (Figure 10b), we found that the band centered on ≈15 cm^{-1} in the marginal spectrum of G^+ (Figure 9) was associated with the fifth IMF (Figure 11c).

In the case of G^+, the situation of the hydration was rather different: For one thing, O1 and O5 did not form the intramolecular H-bond between them because the average value of the O1−O5 distance was 4.67 ± 0.28 Å. For another thing, in roughly 70% of the configurations of our simulation run, O1 and O5 were connected by H-bonded three water molecules

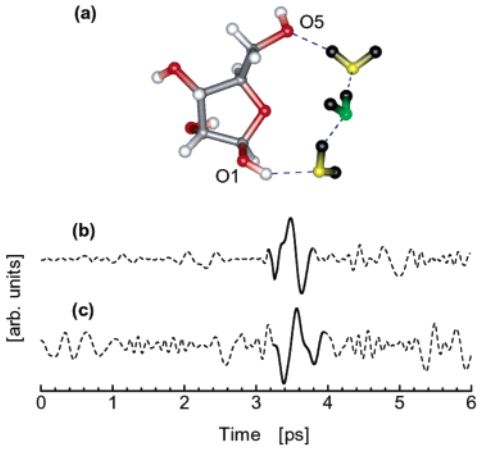

Figure 12. A snapshot taken from the ab initio MD trajectory showing that O1 and O5 of the G^+ rotamer were connected via three H-bonded water molecules (a), the third intrinsic mode function of puckering phase angle for the five-membered circular hydrogen bond network (b), compared with that of ribose puckering (c). In part a, only the three water molecules forming the circular hydrogen bond network are shown and the other water molecules are omitted. Oxygens of the first- and second-hydration-shell water molecules are colored separately by yellow and green with hydrogens black. In the G^+ rotamer of β-ribofuranose, carbon atoms are colored by gray, oxygens red, and hydrogens white. The bold-solid-line-emphasized part of the signal in part b indicates a relatively strong, rapid change in the configuration of the H-bond network, which was accompanied by the similar motion of β-ribofuranose puckering, which is also emphasized by the bold-solid line in part c. The other parts of the signals are denoted by dashed line.

(see Figure 12a), so that the five-membered circular H-bond network was formed (details of this circular H-bond network will be found elsewhere[35]). Since our circular H-bond network is also a five-membered ring, we can define its puckering phase angle. Therefore, we performed the EMD method for this quantity, to shed light on the interaction between the two puckering phase angles of this circular H-bond network and the furanose ring. Comparison of their third IMF suggests that the event centered on ≈3.5 ps of the ribose puckering phase angle (the peak labeled by A in Figure 10) was closely related to the motion of the phase angle of the circular H-bond network (bold-solid lines in Figure 12b and 12c). More specifically, according to the calculation of the cross-correlation function between these IMFs, the motion centered on ≈3.5 ps of the third IMF of the phase angle of ribose puckering appeared to be slightly delayed (roughly ≈0.17 ps) from the original motion of the circular H-bond network. The molecular origin of this event of the circular H-bond network was found to be a relatively strong, rapid change in its phase angle that accompanied the decrease in puckering amplitude (going to a somewhat planar configuration). This implies the transmission of the dynamics from the motion of the circular H-bond network to that of the O1−O5 distance and the phase angle. On the other hand, we could not identify the clear origin for the lower motion of the phase angle of G^+.

In closing, we comment on the interaction between ribofuranose puckering and neighboring water molecules. A simple analysis of the low-frequency region of liquid water by Nakayama[49] showed that the modes associated with the band centered on ≈180 cm^{-1} are mesoscopically distributed in the H-bond network of liquid water whereas the modes associated with the band centered on ≈60 cm^{-1} are strongly localized motions. Moreover, recent molecular dynamics and experimental studies suggested that the latter is more generally found in liquid systems and is associated with restricted translational motions of the local structure of atoms or molecules, resulting in the so-called cage effect.[50,51] Assuming these interpretations and considering both our results and the fact[18] that the major low-frequency fluctuation of puckering occurs at the region below 100 cm^{-1}, we infer that the puckering fluctuation of β-ribofuranose is likely to be created by the localized motions that involve the anomeric and hydroxymethyl oxygens and water molecules near them.

Conclusions

In the present work, we examined the structural fluctuation and the low-frequency dynamics of β-ribofuranose puckering in the N form in aqueous solution, using the method of ab initio MD simulations based on density functional theory. Our analysis suggests that the O1−O5 distance is a simple relevant geometrical parameter that dynamically correlates with the phase angle of the N conformer of β-ribofuranose in aqueous solution: the phase angle rotates clockwise in the pseudorotation cycle when the O1−O5 distance becomes longer. The time-frequency analysis by the HHT also confirmed the correlation. Since the flexibility of the five-membered ring probably depends on furanoses[17] and their conformations, the correlation could be also quantitatively different depending on furanoses and their conformations. Moreover, the correlation may have implications for the transitions between the N and S conformers in aqueous solution.

Our analysis of the ab initio MD trajectories suggests that the molecular origin of the hydration effects on the structural fluctuation and the low-frequency dynamics of β-ribofuranose puckering is closely related to the above correlation and thus primarily attributed to the relatively local interactions among the anomeric and hydroxymethyl groups and the surrounding water molecules: In the G^- rotamer, the low-frequency dynamics of β-ribofuranose puckering was primarily created by the interplay between intra- and intermolecular H-bonds involving the two oxygens, partly because intra- and intermolecular H-bonds were mutually competitive. In the G^+ rotamer, the dynamics of β-ribofuranose puckering appeared to be partially correlated with the motion of the circular H-bond network involving O1, O5, and three water molecules. The difference in the low-frequency dynamics between the two rotamers was reflected in the Fourier spectra and the marginal Hilbert−Huang spectra for the phase angle, and most of the instantaneous frequencies of the phase angle were concentrated on the region below ≈100 cm^{-1}, in agreement with the previous study.[18] While we note the limitations of the present simulations, such as the length of our simulation run, the system size, the conformation, and the performance of density functional theory combined with the BLYP functional, our analysis presented here would provide a better insight into the mechanism of how the hydration affects the low-frequency dynamics of the furanose puckering.

Acknowledgment. Our ab initio MD simulations were performed on a Hitachi SR8000 of Information Technology Center, University of Tokyo.

Supporting Information Available: Correlation coefficients between the phase angle and the structural parameters (the angles belonging to the five-membered ring, Table S1; the bond distances belonging to the five-membered ring, Table S2; the torsional angles of the hydroxymethyl group and the hydroxyl ones, Table S3). This material is available free of charge via the Internet at http://pubs.acs.org.

References and Notes

(1) Altonoa, C.; Sundaralingam, M. *J. Am. Chem. Soc.* **1972**, *94*, 8205.
(2) Cremer, D.; Pople, J. A. *J. Am. Chem. Soc.* **1975**, *97*, 1354.
(3) Rao, S. T.; Westhof, E.; Sundaralingam, M. *Acta Crystallogr. Sect. A* **1981**, *37*, 421.
(4) Altonoa, C.; Sundaralingam, M. *J. Am. Chem. Soc.* **1973**, *95*, 2333.
(5) Serianni. A. S.; Chipman, D. M. *J. Am. Chem. Soc.* **1987**, *109*, 5297.
(6) Kline, P. C.; Serianni, A. S. *J. Am. Chem. Soc.* **1990**, *112*, 7373.
(7) Podlasek, C. A.; Stripe, W. A.; Carmichael, I.; Shang, M.; Basu, B.; Serianni, A. S. *J. Am. Chem. Soc.* **1996**, *118*, 1413.
(8) Church, T. J.; Carmichael, I.; Serianni, A. S. *J. Am. Chem. Soc.* **1997**, *119*, 8946.
(9) Kennedy, J.; Wu, J.; Drew, K.; Carmichael, I.; Serianni, A. S. *J. Am. Chem. Soc.* **1997**, *119*, 8933.
(10) Brameld, K. A.; Goddard, W. A., III. *J. Am. Chem. Soc.* **1999**, *121*, 985.
(11) Gordon, M. T.; Lowary, T. L.; Hadad, C. M. *J. Am. Chem. Soc.* **1999**, *121*, 9682.
(12) Coloran, F.; Zhu, Y.; Osborn, J.; Carmichael, I.; Serianni, A. S. *J. Am. Chem. Soc.* **2000**, *122*, 6435.
(13) Cloran, F.; Carmichael, I.; Serianni, A. S. *J. Am. Chem. Soc.* **2001**, *123*, 4781.
(14) Harvey, S. C.; Prabhakaran, M. *J. Phys. Chem.* **1987**, *91*, 4799.
(15) Van Eijck, B. P.; Kroon, J. *J. Mol. Struct.* **1989**, *195*, 133.
(16) Plavec, J.; Tong, W.; Chattopadhyaya, J. *J. Am. Chem. Soc.* **1993**, *115*, 9734.
(17) Tomimoto, M.; Go, N. *J. Phys. Chem.* **1995**, *99*, 563.
(18) Gabb, H. A.; Lavery, R.; Prévost, C. *J. Comput. Chem.* **1995**, *16*, 667.
(19) Grůza, J.; Koča, J.; Pérez, S.; Imberty, A. *J. Mol. Struct. (THEOCHEM)* **1998**, *424*, 269.
(20) Dejaegere, A. P.; Case, D. A. *J. Phys. Chem. A* **1998**, *102*, 5280.
(21) Houseknecht, J. B.; McCarren, P. R.; Lowary, T. L.; Hadad, C. M. *J. Am. Chem. Soc.* **2001**, *123*, 8811.
(22) Guler, L. P.; Yu, Y.-Q.; Kenttämaa, H. I. *J. Phys. Chem. A* **2002**, *106*, 6754.
(23) Houseknecht, J. B.; Altona, C.; Hadad, C. M.; Lowary, T. L. *J. Org. Chem.* **2002**, *67*, 4647.
(24) Boero, M.; Terakura, K.; Tateno, M. *J. Am. Chem. Soc.* **2002**, *124*, 8949.
(25) (a) Car, R.; Parrinello, M. *Phys. Rev. Lett.* **1985**, *55*, 2471. (b) Parrinello, M. *Solid State Commun.* **1997**, *102*, 107. (c) Marx, D.; Hutter, J. In *Modern Methods and Algorithms of Quantum Chemistry*; Grotendorst, J., Ed.; NIC, FZ: Jülich, 2000; pp 301−449; see also http://www.theochem-.ruhr-uni-bochum.de/research/marx/cprev.en.html.
(26) (a) Sprik, M.; Hutter, J.; Parrinello, M. *J. Chem. Phys.* **1996**, *105*, 1142. (b) Silvestrelli, P. L.; Bernasconi, M.; Parrinello, M. *Chem. Phys. Lett.* **1997**, *277*, 478. (c) Marx, D.; Tuckerman, M. E.; Hutter, J.; Parrinello, M. *Nature* **1999**, *397*, 601. (d) Geissler, P. L.; Dellago, C.; Chandler, D.; Hutter, J.; Parrinello, M. *Science* **2001**, *291*, 2121. (e) Tuckerman, M. E., Marx, D.; Parrinello, M. *Nature* **2002**, *417*, 925. (f) Chen, B.; Ivanov, I.; Klein, M. L.; Parrinello, M. *Phys. Rev. Lett.* **2003**, *91*, 215503. See also references cited in c−f.
(27) Huang, N. E.; Shen, Z.; Long, S. R.; Wu, M. C.; Shih, H. H.; Zheng, Q. N.; Yen, N.-C.; Tung, C. C.; Liu, H. H. *Proc. R. Soc. London A* **1998**, *458*, 903.
(28) We used CPMD version 3.7, (IBM Corp, 1990−2003 and Max-Plank-Institut für Festkörperforshung Stuttgart, 1997−2001), developed by J. Hutter et al.
(29) Tuckerman, M. E.; Parrinello, M. *J. Chem. Phys.* **1994**, *101*, 1302.
(30) For detailed discussions about the fictitious electronic mass, see: (a) Grossman, J. C.; Schwegler, E.; Draeger, E. W.; Gygi, F.; Galli, G. *J. Chem. Phys.* **2004**, *120*, 300. (b) Kuo, I.-F. W.; Mundy, C. J.; McGrath, M. J.; Siepmann, J. I.; VandeVondele, J.; Sprik, M.; Hutter, J.; Chen, B.; Klein, M. L.; Mohamed, F.; Krack, M.; Parrinello, M. *J. Phys. Chem. B* **2004**, *108*, 12990.
(31) (a) Hohenberg, P.; Kohn, W. *Phys. Rev.* **1964**, *136*, B864. (b) Kohn, W.; Sham, L. J. *Phys. Rev.* **1965**, *140*, A1133. (c) Parr, R. G.; Yang, W. In *Density-Functional Theory of Atoms and Molecules*; Breslow, R.; Goodenough, J. B.; Halpern, J.; Rowlingson, J. S. Eds.; The International Series of Monographs on Chemistry, No. 16; Oxford University Press: New York, 1989.
(32) (a) Becke, A. D. *Phys. Rev. A* **1988**, *38*, 3098. (b) Lee, C.; Yang, W.; Parr, R. G. *Phys. Rev. B* **1988**, *37*, 785.
(33) Goedecker, S.; Teter, M.; Hutter, J. *Phys. Rev. B* **1996**, *54*, 1703.
(34) Martyna, G. J.; Klein, M. L.; Tuckerman, M. E. *J. Chem. Phys.* **1992**, *97*, 2635.
(35) Suzuki, T.; Sota, T., submitted to *J. Phys. Chem. B.*
(36) Huang, N. E.; Shen, Z.; Long, S. R. *Annu. Rev. Fluid Mech*. **1999**, *31*, 417.
(37) (a) Lai, Y.-C. *Phys. Rev. E* **1998**, *58*, R6911. (b) Lai, Y.-C.; Armbruster, D.; Kostelich, E. J. *Phys. Rev.* E **2000**, *62*, R29.
(38) Phillips, S. C.; Gledhill, R. J.; Essex, J. W.; Edge, C. M. *J. Phys. Chem. A* **2003**, *107*, 4869.
(39) Cummings, D. A. T.; Irizarry, R. A.; Huang, N. E.; Endy, T. P.; Nisalak, A.; Ungchusak, K.; Burke, D. S. *Nature* **2004**, *427*, 344.
(40) Cui, W.; Li, F.; Allinger, N. L. *J. Am. Chem. Soc.* **1993**, *115*, 2943.
(41) Harvey, S. C.; Prabhakaran, M. *J. Am. Chem. Soc.* **1986**, *108*, 6128.
(42) Pagliai, M.; Raugei, S.; Cardini, G.; Schettino, V. *J. Mol. Struct. (THEOCHEM).* **2003**, *630*, 141.
(43) Leroux, B.; Bizot, H.; Brady, J. W.; Tran, V. *Chem. Phys.* **1997**, *216*, 349.
(44) Molteni, C.; Parrinello, M. *J. Am. Chem. Soc.* **1998**, *120*, 2168.
(45) Kirschner, K. N.; Woods, R. J. *Proc. Natl. Acad. Sci. U.S.A.* **2001**, *98*, 10541.
(46) Klein, R. A. *J. Am. Chem. Soc.* **2002**, *124*, 13931.
(47) Suzuki, T.; Sota, T. *J. Chem. Phys.* **2003**, *119*, 10133.
(48) Hwang, P. A.; Huang, N. E.; Wang, D. W. *Appl. Ocean Res.* **2003**, *25*, 187.
(49) Nakayama, T. *Phys. Rev. Lett.* **1998**, *80*, 1244.
(50) (a) Padró, J. A.; Martí, J. *J. Chem. Phys.* **2003**, *118*, 452. (b) De Santis, A.; Ercoli, A.; Rocca, D. J. *J. Chem.* Phys. **2004**, *120*, 1657. (c) Padró, J. A.; Martí, J. *J. Chem. Phys.* **2004**, *120*, 1659.
(51) Idrissi, A.; Longelin, S.; Sokoliæ, F. *J. Phys. Chem. B* **2001**, *105*, 6004.
(52) (a) Laaksonen, L. *J. Mol. Graph.* 1992, *10*, 33. (b) Bergman, D. L.; Laaksonen, L.; Laaksonen, A. *J. Mol. Graphics Modell.* **1997**, *15*, 301; see also http://www.csc.fi/gopenmol.
(53) Kay, S. M.; Marple, S. T., Jr. *Proc. IEEE.* **1981**, *69*, 1380.